Conference Proceedings

Solar World Congress 2015
Daegu, Korea, 08 – 12 November 2015

Electrical PV Array Reconfiguration Strategy against Partial Shading

Robert Alfie S. Peña[1,2], Erees Queen B. Macabebe[1] and Davide Del Col[2]

[1] Department of Electronics, Computer, and Communications Engineering, School of Science and Engineering, Ateneo de Manila University, Quezon City 1108, Philippines

[2] Dipartimento di Ingegeneria Industriale, Università degli Studi di Padova, Padova 35131, Italy

Abstract

Partial shading presents a huge problem for photovoltaic (PV) arrays because of mismatch losses. One way to maximize power output is to make the arrays dynamic. These dynamic PV arrays change configuration depending on shading pattern and strength. This work evaluates the electrical PV array reconfiguration (EAR) strategy in dynamic arrays that use total-cross tied topology through modeling and simulation. The approach searches for the optimum configuration which has the most equal row irradiance averages. A static 3×3 PV array model and a dynamic PV array model, which uses the EAR algorithm, were developed. The models were tested for binary- and random-irradiance shading. Results show that the EAR strategy suits some shading patterns and that the irradiance distribution affects improvement in power output. The simulations performed demonstrate both the limitations and benefits of using the EAR strategy in PV array reconfiguration.

Keywords: *electrical PV array reconfiguration, dynamic PV array, partial shading, simulation*

1. Introduction

Partial shading in photovoltaic (PV) arrays causes losses in power output. The different irradiance levels produce different current values. Thus, when modules exposed to different irradiance levels are connected in series, the total current is limited by the module with the lowest generated current. This mismatch in current can be reduced when other array topologies are used such as total cross-tied configuration (TCT). However, even with such change, different values for row currents still produce mismatch. Thus, dynamic PV arrays are introduced.

This paper explores dynamic reconfiguration in PV arrays with a view toward its use in smart PV systems that dynamically respond to partial shading. Companies like Trina Solar, SolarEdge, Enphase Energy, and Optistring already offer smart PV modules that mitigate mismatch due to nonuniform irradiance. These solutions are based on a hybrid power conversion architecture, where each PV module has either a power optimizer or a microinverter to obtain the maximum power from a partially shaded array (Burger et al., 2010; La Manna et al., 2014; MacAlpine et al., 2013). While these commercial, smart PV modules compete with dynamic PV arrays at the array level, these technologies can complement one another if reconfiguration is applied at the PV cell level to create a dynamically reconfigurable PV module. A power optimizer or a microinverter can then be attached to the module for coupling at the array level to reduce mismatch to a minimum.

The focus of this work is on a strategy for reconfiguration known as the electrical PV array reconfiguration strategy (EAR). The average improvement in power output is estimated and comparison of power output of static and dynamic arrays to determine power output improvement using the EAR strategy is accomplished through simulation using the popular one-diode PV model.

doi:10.18086/swc.2015.05.14 Available at http://proceedings.ises.org

2. Photovoltaic array model

2.1 One-diode PV cell model

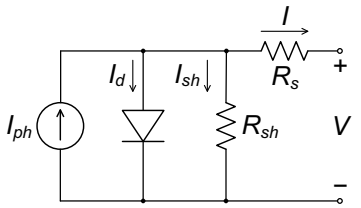

Fig. 1: Circuit representation of the one-diode PV model

One of the popular models that describes a PV cell is the one-diode model. The equivalent circuit of the model is shown in Fig. 1. It is composed of a current source representing the cell's photo-generated current I_{ph}, a single diode connected in parallel, a shunt resistance R_{sh} also connected in parallel and a series resistance R_s (Villalva et al., 2009). A two-diode model is more accurate, but accuracy is obtained at the expense of additional computation. Also, for crystalline silicon PV modules, the one-diode model is sufficient.

The equation describing the model is an expression for the current produced by the PV cell. Looking at the circuit in Fig. 1, the cell current I is just the algebraic sum of the currents of the upper node. Eq. 1 is called the characteristic or the I-V equation of the PV cell:

$$I = I_{ph} - I_{sat}\left(\exp\left(\frac{q(V+IR_s)}{n_d kT}\right)-1\right) - \frac{V+IR_s}{R_{sh}} \qquad \text{(Eq. 1)}$$

where I_{sat} is the diode's reverse saturation current, q is the elementary charge constant, n_d is the diode's ideality factor, k is the Boltzmann constant and T (K) is the absolute temperature of the cell p-n junction. The three terms correspond to the three currents that comprise the cell current: I_{ph}, I_d and I_{sh}. The second term is Shockley's equation for the diode current I_d, where the diode voltage $V_d = V + IR_s$. The third term represents leakage current due to junction defects as represented by the shunt resistance, I_{sh}, obtained by the application of Ohm's law.

2.2 Improved one-diode PV cell model

A serious problem that the classical one-diode model presents, at least for the purposes of this study, is its inadequacy in modeling what happens when a PV cell or module is reverse-biased. This happens when a module or an array is partially shaded. In a series-connected array, the PV module operating in the worst conditions dictates the performance of the whole array (La Manna et al., 2014). A PV cell or module breaks down when the reverse-bias voltage reaches the breakdown voltage (V_{br}) (Alonso-García et al., 2006). To resolve this, the model is modified to account for the avalanche breakdown phenomenon by describing the breakdown phenomenon in the expression for I_{sh} (Orozco-Gutierrez et al., 2014, 2013).

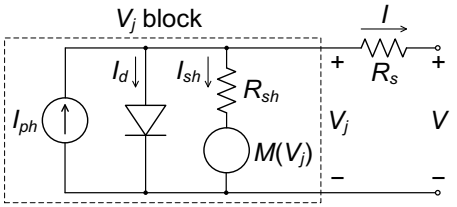

Fig. 2: Circuit representation of the modified one-diode PV model that considers behavior of PV cells in reverse bias

Fig. 2 shows the modified one-diode model equivalent circuit used in this study. Circuit components which are in parallel were lumped into a junction block. This junction block has V_j as its voltage which is equal to V_d. The component $M(V_j)$ represents the modification to the model which takes into account avalanche breakdown in PV cells or modules in reverse bias such that $I_{sh} = V_j M(V_j)/R_{sh}$ (Bishop, 1988). It considers the current through the shunt resistance as mainly the one affected by avalanche breakdown. While the primary

currents are the ones carrying the avalanche effects in other models for cells in reverse bias and parameters were sometimes meaningless or out of range as predicted by theory, the simplicity, wide use and the good fit with actual measurements of this model were instead considered here (Alonso-García and Ruíz, 2006). The modified cell model is:

$$I = I_{ph} - I_{sat}\left(\exp\left(\frac{qV_j}{n_d kT}\right)-1\right) - \frac{V_j}{R_{sh}}\left(1+\alpha\left(1-\frac{V_j}{V_{br}}\right)^{-m}\right) \quad \text{(Eq. 2)}$$

where the additional variables included are α which is the fraction of ohmic current involved in avalanche breakdown exponent, V_{br} which is the junction breakdown voltage when a cell or module is reverse-biased and m which is the avalanche breakdown exponent (Bishop, 1988; Orozco-Gutierrez et al., 2014).

To complete the model, expressions for the other parameters must also be found. What has been described so far is the general characteristic *I-V* equation of a PV module. This equation depends on two parameters: I_{ph} and I_{sat}. Eqs. 3 and 4 are the formulas for I_{ph}:

$$I_{ph,STC} = \frac{R_s + R_{sh}}{R_{sh}} I_{sc,STC} \quad \text{(Eq. 3)}$$

$$I_{ph} = \left(I_{ph,STC} + K_I \Delta T\right)\frac{G}{G_{STC}} \quad \text{(Eq. 4)}$$

where I_{sc} (A) is the module's short-circuit current, K_I (A K^{-1}) is the temperature coefficient of the short-circuit current and G (W m^{-2}) is the irradiance that the module receives. The formulas for I_{sat}, on the other hand is Eq. 5 (Mäki and Valkealahti, 2012):

$$I_{sat} = \frac{I_{ph} - \dfrac{V_{oc,STC} + K_V \Delta T}{R_{sh}}}{\exp\left(\dfrac{V_{oc,STC} + K_V \Delta T}{n_d V_t}\right)-1} \quad \text{(Eq. 5)}$$

where V_{oc} (V) is the module's open-circuit voltage and K_V (V K^{-1}) is the temperature coefficient of the open-circuit voltage (Villalva et al., 2009). The STC in the subscripts of some of the variables refers to the standard testing conditions which specify that junction temperature should be 25 °C, irradiance, 1,000 W m^{-2} and air mass AM 1.5 when measurements are made.

2.3 3×3 PV array with bypass diodes model

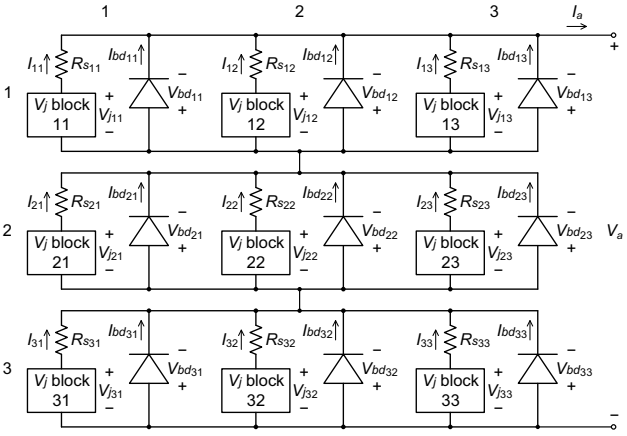

Fig. 3: Circuit representation of the PV array model

To demonstrate the construction of the PV array model, a 3×3 PV array is considered and is shown in Fig. 3. The modules are named according to their position in the array. For example, the module in the second row,

first column of the array is referred to as module 21. In general, for an $M\times N$ array, a module mn has $m\in\{1,2,3,\ldots,M\}$ as its row position and $n\in\{1,2,3,\ldots,N\}$ as its column position. The voltages, currents and resistances are numbered following the designation of the module e.g. V_{11}, V_{j11}, I_{11}, R_{s11} for module 11. Every module has a bypass diode attached to it in antiparallel position. The bypass diodes' voltages and currents also follow the designation of the module it is paired to e.g. V_{bd11}, I_{bd11} for module 11. The array circuit has 18 unique components consisting of nine modules and nine bypass diodes. Thus, the solution requires 18 voltage variables. These variables are stored in a vector called **x**. In general, for an $M\times N$ array, $\mathbf{x} = [V_{j11}V_{bd11}V_{j12}V_{bd12}\cdots V_{jMN}\,V_{bdMN}]^{\mathrm{T}}$, which contains MN variables.

To create the system of equations that describes the 3×3 PV array in Eq. 6, Kirchhoff's voltage and current laws (KVL and KCL) are applied to the circuit in Fig. 3. The 18 variables require that the system of equations consist of 18 equations. There are three rows in the array, so the system of equations can be split into three divisions, one division for each row, each division containing six equations. Each division has the same form, except for the last one. For the first division, the procedure is to first apply KVL to the five meshes in the array's first row. The convention chosen is such that meshes follow the clockwise direction. For the first mesh, $V_{j11}-I_{11}(V_{j11})R_{s11} + V_{bd11} = 0$. The same steps are done for the remaining four meshes. To obtain the last equation in the division, KCL is applied to the node connecting the array's first and second rows. The convention is chosen such that currents leaving the node are positive. The converse is true for currents entering the node. Thus, $\sum_{n=1}^{N}\left[I_{1n}\left(V_{j_{1n}}\right)+I_{bd_{1n}}\left(V_{bd_{1n}}\right)\right]-\sum_{n=1}^{N}\left[I_{2n}\left(V_{j_{2n}}\right)+I_{bd_{2n}}\left(V_{bd_{2n}}\right)\right]=0$. The same procedure was followed for the other divisions. However, the last equation of the third division differs because it is the application of KVL to the big mesh containing the array voltage V_a.

$$\mathbf{F}(\mathbf{x})=\begin{cases}
V_{j_{11}}-I_{11}\left(V_{j_{11}}\right)R_{s_{11}}+V_{bd_{11}}=0\\
-V_{bd_{11}}-V_{j_{12}}+I_{12}\left(V_{j_{12}}\right)R_{s_{12}}=0\\
V_{j_{12}}-I_{12}\left(V_{j_{12}}\right)R_{s_{12}}+V_{bd_{12}}=0\\
-V_{bd_{12}}-V_{j_{13}}+I_{13}\left(V_{j_{13}}\right)R_{s_{13}}=0\\
V_{j_{13}}-I_{13}\left(V_{j_{13}}\right)R_{s_{13}}+V_{bd_{13}}=0\\
\sum_{n=1}^{N}\left[I_{1n}\left(V_{j_{1n}}\right)+I_{bd_{1n}}\left(V_{bd_{1n}}\right)\right]-\sum_{n=1}^{N}\left[I_{2n}\left(V_{j_{2n}}\right)+I_{bd_{2n}}\left(V_{bd_{2n}}\right)\right]=0\\
V_{j_{21}}-I_{21}\left(V_{j_{21}}\right)R_{s_{21}}+V_{bd_{21}}=0\\
-V_{bd_{21}}-V_{j_{22}}+I_{22}\left(V_{j_{22}}\right)R_{s_{22}}=0\\
V_{j_{22}}-I_{22}\left(V_{j_{22}}\right)R_{s_{22}}+V_{bd_{22}}=0\\
-V_{bd_{22}}-V_{j_{23}}+I_{23}\left(V_{j_{23}}\right)R_{s_{23}}=0\\
V_{j_{23}}-I_{23}\left(V_{j_{23}}\right)R_{s_{23}}+V_{bd_{23}}=0\\
\sum_{n=1}^{N}\left[I_{2n}\left(V_{j_{2n}}\right)+I_{bd_{2n}}\left(V_{bd_{2n}}\right)\right]-\sum_{n=1}^{N}\left[I_{3n}\left(V_{j_{3n}}\right)+I_{bd_{3n}}\left(V_{bd_{3n}}\right)\right]=0\\
V_{j_{31}}-I_{31}\left(V_{j_{31}}\right)R_{s_{31}}+V_{bd_{31}}=0\\
-V_{bd_{31}}-V_{j_{32}}+I_{32}\left(V_{j_{32}}\right)R_{s_{32}}=0\\
V_{j_{32}}-I_{32}\left(V_{j_{32}}\right)R_{s_{32}}+V_{bd_{32}}=0\\
-V_{bd_{32}}-V_{j_{33}}+I_{33}\left(V_{j_{33}}\right)R_{s_{33}}=0\\
V_{j_{33}}-I_{33}\left(V_{j_{33}}\right)R_{s_{33}}+V_{bd_{33}}=0\\
-V_{bd_{13}}-V_{bd_{23}}-V_{bd_{33}}-V_a=0
\end{cases} \qquad \text{(Eq. 6)}$$

Eq. 2, the characteristic *I-V* equation, was used to compute for values of $I_{mn}(V_{jmn})$ in the system of equations. On the other hand, the Shockley diode equation in Eq. 7 was used to compute for values of $I_{bd}(V_{bdmn})$ in the system of equations:

$$I = I_{sat,bd}\left(\exp\left(\frac{qV_{bd}}{n_{bd}kT}\right)-1\right) \qquad \text{(Eq. 7)}$$

The mesh used to obtain the last equation in the system is especially chosen to create the Jacobian matrix **J**

of the vectorial function **F** with a diagonal containing nonzero elements. The Jacobian matrix is needed to use Newton's method for systems of nonlinear equations. In Newton's method, the equation $\mathbf{J}(\mathbf{x}_i)\Delta\mathbf{x} = -\mathbf{F}(\mathbf{x}_i)$ is solved for $\Delta\mathbf{x}$. Then, this vector is substituted in $\mathbf{x}_{i+1} = \mathbf{x}_i + \Delta\mathbf{x}$ for the new value **x**. There is an initial guess $\mathbf{x}_0$ that serves as the initial value of **x**. The two steps are repeated until convergence. In theory however, a convergent Newton's method is reached only after an infinite number of iterations. In practice, a tolerance that is small enough for one's purpose is set (Quarteroni and Saleri, 2006).

One important step in Newton's method is the choice of the initial approximation $\mathbf{x}_0$. The convergence of the method depends on it. The choice of $\mathbf{x}_0$ must be sufficiently close to the actual solution for Newton's method to converge (Quarteroni and Saleri, 2006). As stated earlier, V_a is swept from V_{oc} to zero. The actual value of the array's V_{oc} is unknown, so an approximate value for the modules' V_{oc}, solved using Eq. 8, is used (Orozco-Gutierrez et al., 2014):

$$V_{oc,init} = V_t n_d \ln\left(1 + \frac{I_{ph}}{I_{sat}}\right) \qquad \text{(Eq. 8)}$$

Assuming that the modules in the array have the same material properties and are under the same conditions, the array's V_{oc} is just a module's V_{oc} multiplied by the number of rows m. Another use of Eq. 8 is in populating the initial approximation $\mathbf{x}_0$. Because of the parallel connection, a module and the bypass diode connected to it always have the same voltage. So, $\mathbf{x}_0 = [V_{oc,init} V_{oc,init} \cdots V_{oc,init}]^T$.

2.4 3×3 PV array with bypass diodes program

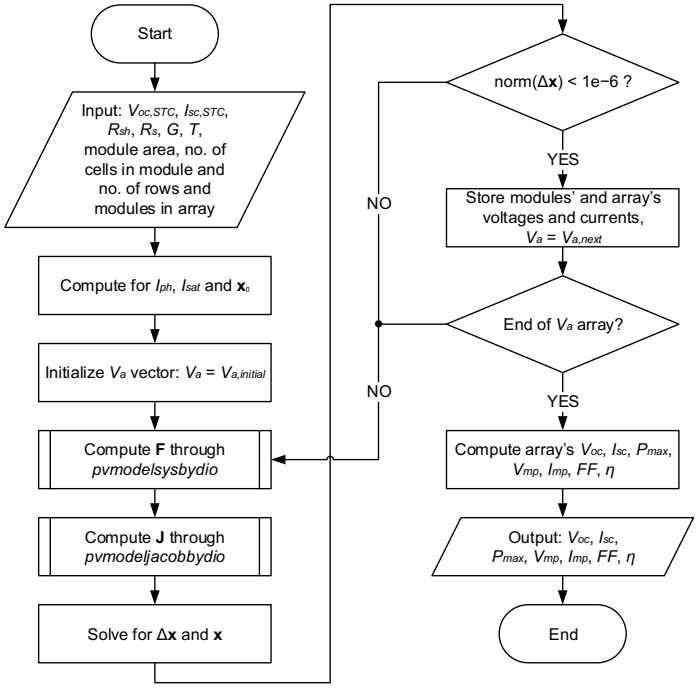

Fig. 4: Flowchart of the MATLAB function *pvmodelbydio*

The equations and the model described in the previous sections were programmed in MATLAB. They were incorporated into the function *pvmodelbydio*, shown in Fig. 4. The function takes G, the module's surface area and the number of rows and modules in the array as inputs or arguments. On the other hand, the outputs are the array's V_{oc}, I_{sc}, P_{max}, V_{mp}, I_{mp}, fill factor (FF) and efficiency (η) under given conditions. The conditions are dictated by the irradiance G that each module receives and the temperature of the module T. In the function, however, only G is an input. Module temperatures were set at 35, 45 and 55 °C. When the function is called, the program computes for I_{ph} and I_{sat} of all the modules in the array using Eqs. 4 and 5. $V_{oc,init}$ is also computed using Eq. 8 and is used to populate the initial approximation $\mathbf{x}_0$. Eq. 8 is also used to initialize the MATLAB vector for V_a from its approximate V_{oc} value to zero. Newton's method is applied

starting with the first element of the vector. It is repeated until a condition is reached that causes termination of Newton's method. In this case, termination is set when the norm of $\Delta\mathbf{x}$ reaches a tolerance of 1×10^{-6}. Thus, the system is solved for the first value of V_a. The steps are repeated for the next values of the array voltage. The whole process is akin to setting the array voltage at a specific level, and finding out the values of all the parameters of interest. To completely characterize the system then is to sweep the voltage from its open-circuit value down to zero and solving the resulting systems of equations.

3. Reconfiguration strategies and their simulation

Velasco-Quesada et al. proposed a scheme for the reconfiguration of PV arrays to minimize mismatch and therefore maximize power output (Velasco-Quesada et al., 2009). They called this the electrical array reconfiguration or EAR strategy. It is based on the principle of irradiance equalization that their group earlier explored (Velasco et al., 2005).

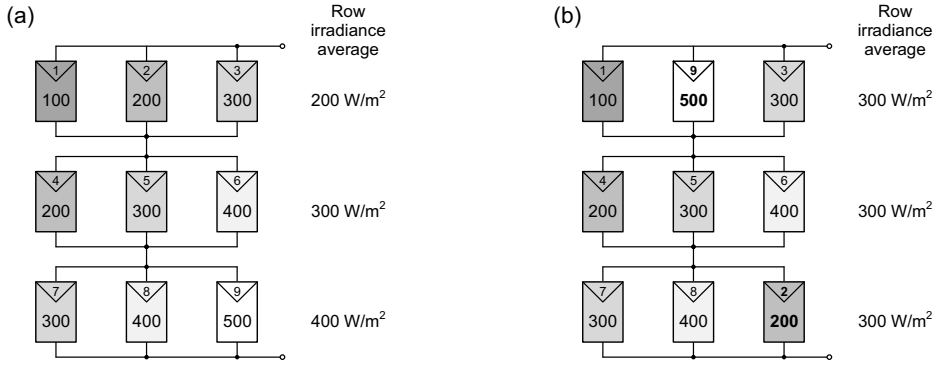

Fig. 5: Principle of irradiance equalization for dynamic PV arrays: (a) original configuration and (b) new configuration where modules 2 and 9 were interchanged

Irradiance equalization serves as a framework for the reconfiguration strategy for PV arrays in TCT configuration tested in this work. It works by configuring PV arrays in such a way that each row's average irradiance is as close as possible to the average irradiances of the other rows. The principle is illustrated with an idealized example in Fig. 5. Fig. 5(a) is the original configuration. In irradiance equalization, the configuration that minimizes the difference among the average row irradiances becomes the new configuration. Fig. 5(b) is such a configuration. The connections of modules 2 and 9 were interchanged resulting in equal average row irradiances.

Irradiance equalization works because it reduces the current mismatch among the rows which are connected in series. Even though the rows have different shading profiles, they will still produce currents which are close in value to one another because they have close average row irradiances. Previous studies show that cross-tied configurations such as TCT and bridge-link arrays do not only produce more power in the face of partially shadowed conditions but are also more reliable in terms of operational lifetimes as compared to serial-parallel (SP) arrays (Gautam and Kaushika, 2002; Kaushika and Gautam, 2003). The effect of a change in irradiance is mostly seen in the current produced by a PV module. The effect on voltage is minimal (Velasco-Quesada et al., 2009). This makes the parallel connection of modules possible with minimal effect on the current produced by a row. Mismatch still happens, but at the level of the series connection of rows. The array current is limited by the row that produces the lowest current. As already said for modules connected in series, the module in the worst operating conditions dictate the performance of the whole array. By employing irradiance equalization through array reconfiguration, current mismatch is reduced.

3.1 Electrical PV array reconfiguration strategy

As can be observed in the topology of TCT arrays, there are permutations which are equivalent in terms of power production. Cases of two interchanged parallel modules are redundant. Also redundant are interchanged rows in series. Computing for these irrelevant cases is just a waste of time. The EAR strategy discards these redundancies when considering the total number of configurations of interest (COIs) (Velasco-Quesada et al., 2009). For an $M\times N$ array, the number of configurations of interest is:

$$N_{coi} = \frac{(MN)!}{M!(N!)^m} \quad \text{(Eq. 9)}$$

For a 3×3 array where $M = N = 3$, the total number of permutations possible is 9! = 362,880 while the number of COIs given by Eq. 9 is 280. Based on these numbers, it can be seen that considering only the COIs greatly reduces the number of configurations that the EAR algorithm has to consider.

The following are the steps that describe the algorithm to implement the EAR strategy:

1. The COIs are computed based on the size of the PV array.
2. The irradiance of each module in the array is estimated using the voltage and current values of individual modules.
3. For a COI, irradiance values of the modules in each row are averaged. Each row of the COI then has an associated average row irradiance. The same is done for the other COIs.
4. For a COI, an "irradiance equalization index" is computed for based on the average row irradiances. This index is just the difference between the maximum and minimum values among the average row irradiances. The same is done for the other COIs so each has an associated index. The COI with the lowest index becomes the target for the reconfiguration.
5. In case of COIs with equal indices, the tie is broken by computing for the number of module relocations needed to arrive there from the current configuration. The COI with the lowest number of relocations then becomes the target for the reconfiguration.

Table 1: Array sizes and number of configurations

Array size	Total number of configurations	Number of configurations of interest
3×3	362,880	280
4×4	2.09×10^{13}	2,627,625
5×5	1.55×10^{25}	5.19×10^{12}

A problem emerges when scaling is considered. Table 1 shows different array sizes and the corresponding total number of configurations and number of COIs. For a 3×3 array, only 280 COIs have to be considered and for square arrays larger than 3×3, implementation of the EAR strategy becomes harder because of the exponential jump in the number of COIs. This issue is fundamental in the EAR strategy as COIs are the framework for the scheme.

3.2 Simulation and performance tests of the strategies

The EAR algorithm was also implemented in MATLAB. Two models were constructed: a static array and a dynamic array using the EAR strategy. Also, two tests were conducted for the static and dynamic PV array models: binary- and random-irradiance shading. For the binary-irradiance test, 511 shading patterns containing all combinations of shaded modules were generated for each irradiance level. Random-irradiance shading, on the other hand, involved random irradiance values which follow uniform and normal distributions. 1,000 random shading patterns were prepared for both distributions. The simulations were run on desktop PCs with Intel Core i5-3450 (at 3.10 GHz) processors.

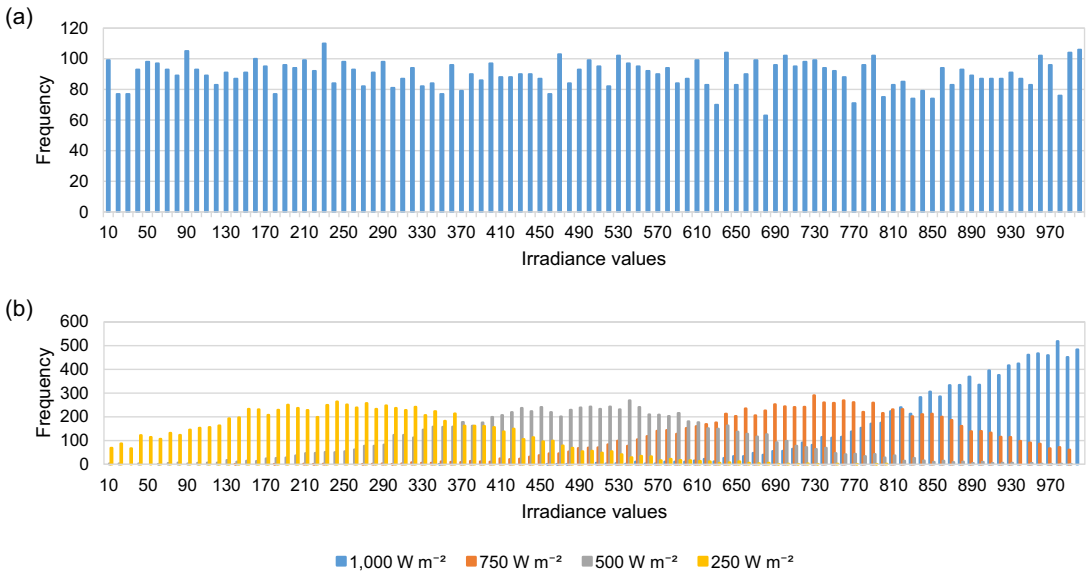

Fig. 6: Histogram of the random irradiance distributions: (a) uniform distribution and (b) normal distributions with different means and σ = 150 W m^{-2}

The histograms for the two random irradiance shading tests are shown in Fig. 6. The uniform distribution in Fig. 6(a) simulates a condition for a PV array where the change in irradiance of each PV module over time is drastic. The normal distribution, on the other hand, simulates a condition where the change in irradiance over time is more moderated or more concentrated within an irradiance range as seen in Fig. 6(b). In actual conditions, it could resemble different levels of cloudy conditions. The different levels are simulated as the means (μ) of the normal distribution: 1,000, 750, 500 and 250 W m^{-2}. A standard deviation (σ) of 150 W m^{-2} was chosen for the distributions. To give an idea of the range of irradiance values this σ brings, for a mean of 500 W m^{-2}, 95% of the values are within 2σ or within the range 200–800 W m^{-2}. 68% of the values are within a σ or within the range 350–650 W m^{-2}. Other values for the standard deviation could also be tested, but the results here are for σ = 150 W m^{-2}. The range of irradiance values was limited to 0–1,000 W m^{-2}.

Table 2: Parameters of the PV module and bypass diode used in the model

Parameter	Value	Parameter	Value
V_{oc}	21.7 V	R_s	1.4 Ω
I_{sc}	0.61 A	R_{sh}	2.31×10^4 Ω
V_{mp}	17.3 V	V_{br}	−15 V
I_{mp}	0.58 A	M	3
P_{max}	10 W	A	0.002
K_V	−0.0708 V K^{-1}	n_d	1.3
K_I	0.0034 A K^{-1}	n_{bd}	1.5
N_s	36	$I_{sat,bd}$	5.6×10^{-6} A

Table 2 gives the parameters used in the model for the PV module and bypass diode. The PV model used in this study is the GP010PA PV module by Alexan Commercial. K_V and K_I were obtained from outdoor experiments characterizing and measuring the performance of the modules. The values for the resistances R_s and R_{sh}, on the other hand, were obtained following the procedure for the modeling of PV modules (Villalva et al., 2009).

4. Results and discussion

The two tests were performed for both the static and dynamic PV arrays to compare their power outputs and ultimately to assess whether using the EAR strategy for dynamic arrays improves power output.

4.1 Binary-irradiance test results

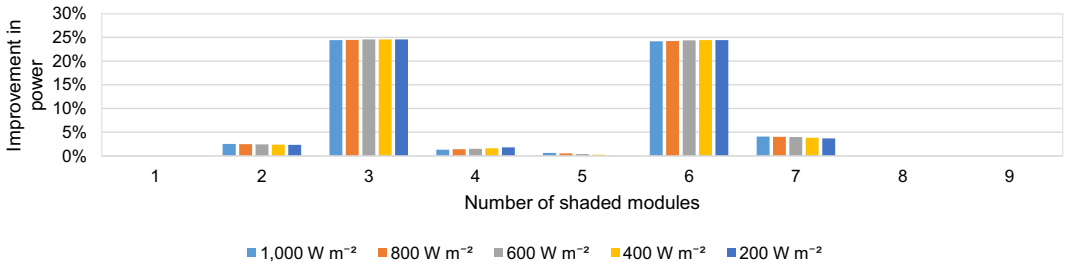

Fig. 7: Average percent improvement in power output of the 3×3 dynamic over the static PV array model in binary-irradiance shading at 35 °C; irradiance of shaded modules is 5% of unshaded level

Fig. 7 shows the results for the binary-irradiance shading test where each PV module in the array can either be shaded or unshaded. Both the static and EAR-based model were run 511 times for each irradiance and shading level. This is based on the total number of combinations possible for shaded and unshaded modules in the array. The unshaded irradiance level in a run can have a value of 1,000, 800, 600, 400 or 200 W m^{-2}, while the shaded irradiance level is 5% of the unshaded level. It can be seen that when a module is shaded and when only one module is unshaded (eight modules are shaded), using a dynamic array based on the EAR strategy does not improve power output. The principle on which the strategy is based, irradiance equalization, cannot optimize these cases. Otherwise, using dynamic arrays improved power output for other cases when the number of shaded modules is not one or eight.

Table 3: Percentage of shading patterns with decreased and increased power output due to the EAR strategy for 1,000 W m^{-2} unshaded irradiance level at 35 °C

No. of shaded modules	Total no. of shading patterns	Patterns with decreased power	Patterns with the same power	Patterns with increased power
1	9	0%	100%	0%
2	36	0%	75%	25%
3	84	0%	32.14%	67.86%
4	126	35.71%	21.43%	42.86%
5	126	47.62%	16.67%	35.71%
6	84	0%	32.14%	67.86%
7	36	0%	75%	25%
8	9	0%	100%	0%

From the results in Fig. 7, it can be observed that the EAR algorithm performs best when the number of shaded modules equals the number of columns in the array or is a multiple of it, as in the case when three and six modules are shaded. It was able to relocate the shaded modules into columns such that each row has the same number of shaded modules as the other rows. Average improvement in power when three modules are shaded (24.39%) in the case of 1,000 W m^{-2} is as much as nine times better than when two modules are shaded (2.53%).

The effect of using the EAR strategy in dynamic arrays on the number of patterns with decreased or increased power output is summarized in Table 3. Percent differences whose absolute value is less than 0.01 were taken to show no difference in power output between the static and dynamic arrays. The table also shows that the decrease in power is only seen when four or five modules are shaded. The case when five

modules are shaded serves as another illustrative example of the limitation of the EAR strategy. For instance, at an array temperature of 35 °C and unshaded irradiance level of 1,000 W m^{-2}, the dynamic array in 47.62% of the 126 shading patterns possible produced a decrease, instead of an increase, in power. This means that for these numbers, the EAR strategy is unable to optimize the power for some shading patterns.

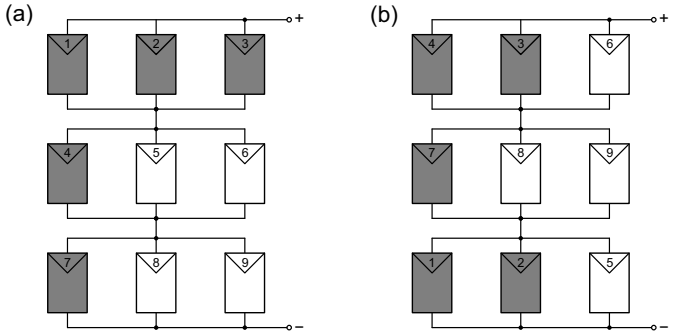

Fig. 8: Third case when five modules are shaded at 35 °C and unshaded irradiance level of 1,000 W m^{-2}: (a) original shading pattern and (b) shading pattern after reconfiguration using the EAR strategy

Fig. 8 shows a sample case of five shaded modules where the EAR strategy failed. The third shading pattern for five shaded modules at 35 °C and unshaded irradiance level of 1,000 W m^{-2} is shown in Fig. 8(a). This original configuration produced a power of 40.06 W. The resulting shading pattern after reconfiguration through the EAR strategy is shown in Fig. 8(b). It has a power of 35.29 W. Fig. 8 is a case of the reconfiguration strategy not being able to optimize a shading pattern. As the power outputs show, applying the EAR strategy reduced the power output instead of improving it. In Fig. 8(a), the whole of the first row is shaded. However, the bypass diodes connected to every panel served as an alternative path for the array current. In effect, the configuration actually has balanced currents. On the other hand, Fig. 8(b) has unbalanced row currents. The second row of this configuration has two unshaded modules, unlike the first and the third rows. The row currents are mismatched resulting in a lower power output as compared to the original configuration in Fig. 8(a).

4.2 Random uniformly distributed irradiance shading test results

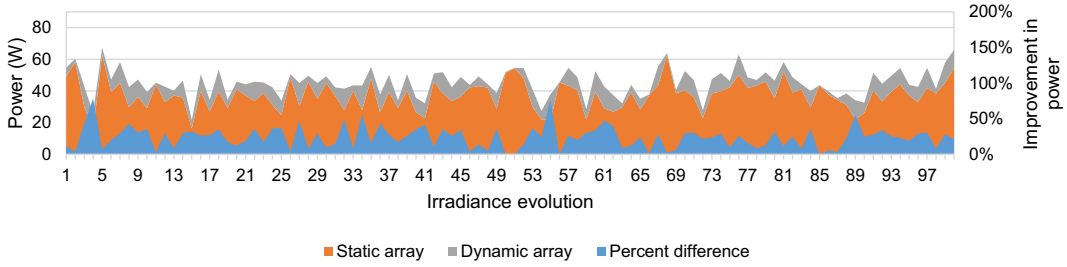

Fig. 9: Power output of 3×3 static and dynamic photovoltaic array models in random-irradiance shading (first 100 shading patterns) with uniformly distributed irradiance at 35 °C

For the first random-irradiance shading test, uniformly distributed shading patterns were generated. The simulation of the models was executed with each pattern as input. Fig. 9 shows the irradiance evolution and the output power for both static and dynamic arrays at 35 °C. The model was run 1,000 times for each distribution because there were 1,000 shading patterns generated for each distribution.

Table 4: Percent improvement in power of the dynamic arrays over the static array with uniformly distributed shading patterns

Improvement at 35 °C	Improvement at 45 °C	Improvement at 55 °C
21.12%	20.87%	20.61%

Table 4 shows the average improvement in power of the EAR-based dynamic over the static array when the irradiances in the shading pattern is uniformly distributed. With uniformly distributed shading patterns, improvements of above 20% can be expected. Percent improvement decreases with an increase in temperature, but the effect of temperature on the percent improvement is very minimal.

4.3 Random normally distributed irradiance shading test results

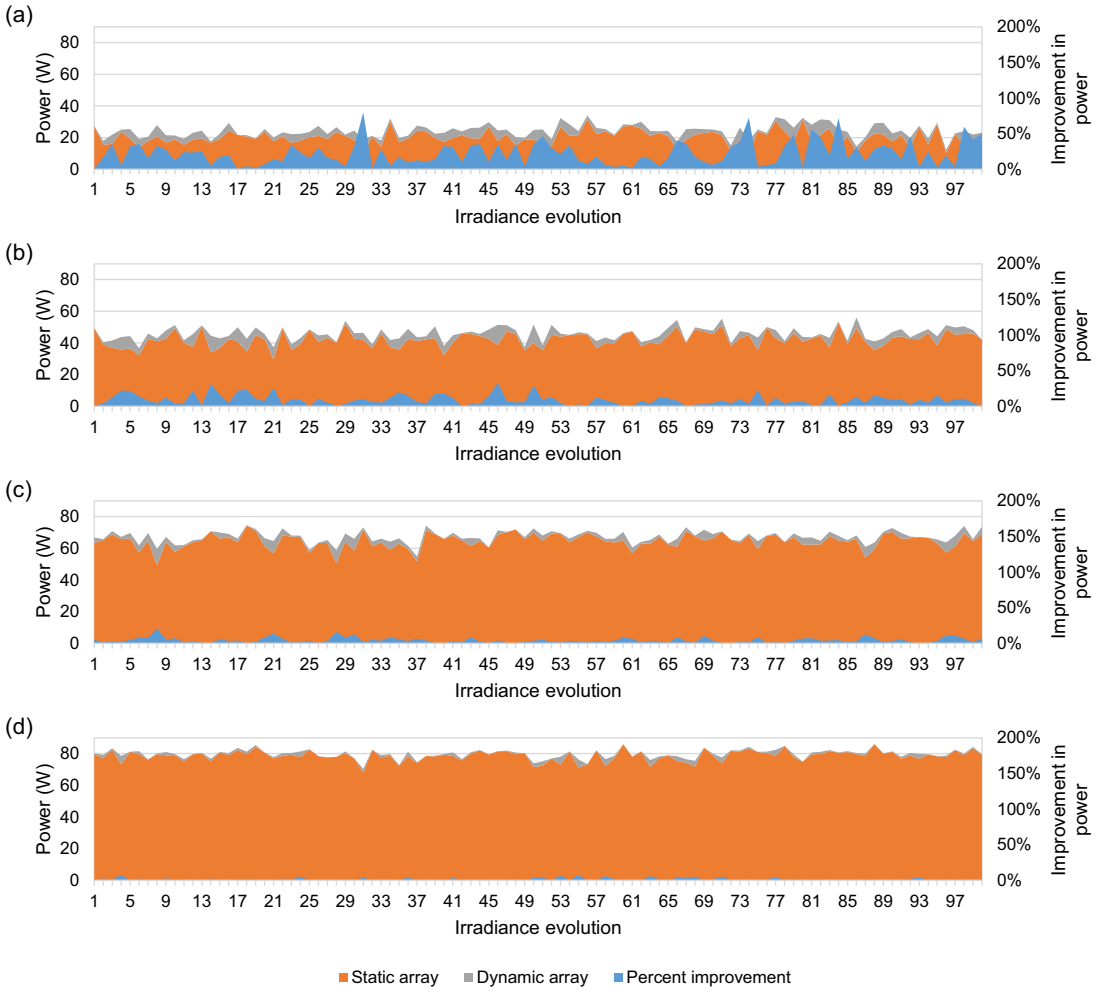

Fig. 10: Power output of 3×3 static and dynamic photovoltaic array models in random-irradiance shading (first 100 shading patterns) at 35 °C with normally distributed irradiance (σ = 150 W m^{-2}): (a) μ = 250 W m^{-2}, (b) μ = 500 W m^{-2}, (c) μ = 750 W m^{-2} and (d) μ = 1,000 W m^{-2}

Fig. 10 shows the results for the second random irradiance shading test with the distributions centered at different irradiances at 35 °C. The irradiance level at 1,000 W m^{-2} was taken as the maximum possible irradiance so the distribution centered at this value is only a half-normal distribution, as in Fig. 6. As seen in Figs. 10(a)–(d), the percent improvement of the dynamic over the static array is small for the irradiance distributions centered at 750 and 1,000 W m^{-2}. The percent improvement increases as the mean of the distribution decreases.

Table 5: Percent improvement in power of the dynamic arrays over the static array with normally distributed shading patterns

Irradiance distribution mean (W m^{-2})	Improvement at 35 °C	Improvement at 45 °C	Improvement at 55 °C
250	20.62%	20.35%	20.06%
500	9.63%	9.37%	9.09%
750	4.13%	3.96%	3.79%
1,000	1.52%	1.43%	1.35%

Table 5 summarizes the results of the random irradiance shading test. The values confirm that as the mean of the distribution increases, the percent improvement decreases. The values for the distribution centered at 250 W m^{-2} almost match those obtained for uniformly distributed irradiances. However, for the other distributions, percent improvement is much less than half that of the uniform distributions. It shows that as the irradiance distribution becomes more spread, the dynamic array becomes more effective in recovering power which is otherwise lost due to partial shading.

It must be noted however, that while the percent improvement is high for lower irradiances, actual deployment of a dynamically reconfigurable array will depend on the power requirements of the system versus the recoverable power, as estimated here. Table 5 also shows the effect of temperature on the percent improvement. As in the uniform distributions, percent improvement minimally increases as the temperature decreases.

5. Conclusion

This work demonstrates some of the limitations and benefits in using the EAR strategy in dynamic PV arrays through modeling and simulation. The binary-irradiance shading test showed that the algorithm works best for particular configurations. Specifically, irradiance equalization works best when the number of shaded modules equals the number of columns. On the other hand, the random-irradiance shading test revealed how the irradiance distribution affects power output improvement when a dynamic array is used. Dynamic reconfiguration is most effective when the distribution of irradiance each module receives is more uniformly spread. Thus, shading profiles must also be studied if dynamic reconfiguration is to be implemented. The two tests employed here can serve as platforms for evaluating dynamic reconfiguration strategies for PV systems. PV system designers benefit by considering these results that inform when and where to use the EAR strategy in dynamic PV arrays.

6. Acknowledgment

The authors thank the Engineering Research and Development for Technology program of the Philippine Department of Science and Technology (DOST-ERDT) for supporting this work and Erasmus Mundus Mobility with Asia-West 2013 (EMMA-West 2013) for providing R. A. S. Peña with a mobility grant that allowed completion of part of this work at Università degli Studi di Padova.

7. References

Alonso-García, M., Ruíz, J., Chenlo, F., 2006. Experimental study of mismatch and shading effects in the – characteristic of a photovoltaic module. Sol. Energy Mater. Sol. Cells 90, 329–340. doi:10.1016/j.solmat.2005.04.022

Alonso-García, M.C., Ruíz, J.M., 2006. Analysis and modelling the reverse characteristic of photovoltaic cells. Sol. Energy Mater. Sol. Cells 90, 1105–1120. doi:10.1016/j.solmat.2005.06.006

Bishop, J.W., 1988. Computer simulation of the effects of electrical mismatches in photovoltaic cell interconnection circuits. Sol. Cells 25, 73–89. doi:10.1016/0379-6787(88)90059-2

Burger, B., Goeldi, B., Rogalla, S., Schmidt, H., 2010. Module Integrated Electronics–An Overview, in: 25th European Photovoltaic Solar Energy Conference and Exhibition/5th World Conference on Photovoltaic Energy Conversion. Valencia, Spain, pp. 3700–3707. doi:10.4229/25thEUPVSEC2010-4EP.1.1

Gautam, N.K., Kaushika, N.D., 2002. Reliability evaluation of solar photovoltaic arrays. Sol. Energy 72, 129–141. doi:10.1016/S0038-092X(01)00085-8

Kaushika, N.D., Gautam, N.K., 2003. Energy Yield Simulations of Interconnected Solar PV Arrays. IEEE Trans. Energy Convers. 18, 127–134. doi:10.1109/TEC.2002.805204

La Manna, D., Li Vigni, V., Riva Sanseverino, E., Di Dio, V., Romano, P., 2014. Reconfigurable electrical interconnection strategies for photovoltaic arrays: A review. Renew. Sustain. Energy Rev. 33, 412–426. doi:10.1016/j.rser.2014.01.070

MacAlpine, S.M., Erickson, R.W., Brandemuehl, M.J., 2013. Characterization of Power Optimizer Potential to Increase Energy Capture in Photovoltaic Systems Operating Under Nonuniform Conditions. IEEE Trans. Power Electron. 28, 2936–2945. doi:10.1109/TPEL.2012.2226476

Mäki, A., Valkealahti, S., 2012. Power losses in long string and parallel-connected short strings of series-connected silicon-based photovoltaic modules due to partial shading conditions. IEEE Trans. Energy Convers. 27, 173–183. doi:10.1109/TEC.2011.2175928

Orozco-Gutierrez, M.L., Ramirez-Scarpetta, J.M., Spagnuolo, G., Ramos-Paja, C. a., 2014. A method for simulating large PV arrays that include reverse biased cells. Appl. Energy 123, 157–167. doi:10.1016/j.apenergy.2014.02.052

Orozco-Gutierrez, M.L., Ramirez-Scarpetta, J.M., Spagnuolo, G., Ramos-Paja, C.A., 2013. A technique for mismatched PV array simulation. Renew. Energy 55, 417–427. doi:10.1016/j.renene.2013.01.009

Quarteroni, A., Saleri, F., 2006. Scientific Computing with MATLAB and Octave, 2nd editio. ed, Texts in Computational Science and Engineering. Springer Berlin Heidelberg, Berlin, Heidelberg. doi:10.1007/3-540-32613-8

Velasco, G., Negroni, J.J., Guinjoan, F., Pique, R., 2005. Irradiance equalization method for output power optimization in plant oriented grid-connected PV generators, in: 2005 European Conference on Power Electronics and Applications. IEEE, p. 10 pp.–P.10. doi:10.1109/EPE.2005.219300

Velasco-Quesada, G., Guinjoan-Gispert, F., Piqué-López, R., Román-Lumbreras, M., Conesa-Roca, A., 2009. Electrical PV array reconfiguration strategy for energy extraction improvement in grid-connected PV systems. IEEE Trans. Ind. Electron. 56, 4319–4331. doi:10.1109/TIE.2009.2024664

Villalva, M.G., Gazoli, J.R., Filho, E.R., 2009. Comprehensive Approach to Modeling and Simulation of Photovoltaic Arrays. IEEE Trans. Power Electron. 24, 1198–1208. doi:10.1109/tpel.2009.2013862